Structure of excited states of ^{11}Be studied with Antisymmetrized Molecular Dynamics

Y. Kanada-En'yo
Institute of Particle and Nuclear Studies,
High Energy Accelerator Research Organization,
1-1 Oho, Tsukuba, Ibaraki 305-0801, Japan

H. Horiuchi
Department of Physics, Kyoto University, Kyoto 606-01, Japan

Abstract

The structures of the ground and excited states of ^{11}Be were studied with a microscopic method of antisymmetrized molecular dynamics. The theoretical results reproduce the abnormal parity of the ground state and predict various kinds of excited states. We suggest a new negative-parity band with a well-developed clustering structure which reaches high-spin states. Focusing on a 2α clustering structure, we investigated structure of the ground and excited states. We point out that molecular orbits play important roles for the intruder ground state and the low-lying $2\hbar\omega$ states. The features of the breaking of α clusters were also studied with the help of data for Gamow-Teller transitions.

I. INTRODUCTION

Recently, information on the excited states of light unstable nuclei has increased rapidly [1–5]. In the excited states of light unstable nuclei, an exotic molecular structure of light unstable nuclei is one of the attractive subjects in experimental and theoretical research. For example, molecular structure has been suggested to appear in neutron-rich nuclei, such as ^{10}Be and ^{12}Be [1,4–12]. W. Von Oertzen et al. [6,7] proposed a kind of exotic clustering structure with a $2\hbar\omega$ configuration in the excited states of ^{11}Be. However, there have been few microscopic studies on the excited states of ^{11}Be.

Needless to say, α-cluster cores are very important in the ground and excited states of ^{11}Be as well as in ^{9}Be and ^{10}Be. However, we should not forget the breaking of α-clusters in ^{11}Be because there are many valence neutrons around the α-clusters. The experimental data concerning the β-decay strength are very useful to estimate the breaking of the 2α clustering structure in Be isotopes, because Gamow-Teller transitions from Li to Be are not allowed if the α-cluster cores in the daughter state of Be are completely ideal ones with a simple $(0s)^4$ configuration. It is very interesting that the recently measured β-decay strength from ^{11}Li to

^{11}Be indicates significant breaking of α-clusters in the excited states of ^{11}Be [2]. Therefore, it is important to also study the breaking of α-clusters due to the surrounding neutrons as well as the development of clustering in ^{11}Be.

We should point out another interesting feature in ^{11}Be. Abnormal parity of the ground state in ^{11}Be has been known for a long time. Namely, the spin parity of the ground state is $1/2^+$, which seems to be inconsistent with the ordinary shell-model picture in which ^{11}Be with 7 neutrons may have a $1/2^-$ state as the ground state. It has long been a problem why parity inversion occurs in ^{11}Be. As possible reasons for this parity inversion, such effects as the halo structure, a core deformation, clustering and paring are suggested. For example, the energy gain of a positive parity state of ^{11}Be is discussed in Refs [13–17]. However, the ground-state structure has not been sufficiently studied by fully microscopic calculations without such assumptions as the existence of core nuclei. Although the clustering structure must be important in Be isotopes, it is difficult for mean-field approaches to describe developed clustering structures. With a theoretical method of antisymmetrized molecular dynamics, Doté et al. have studied the abnormal parity ground state of ^{11}Be without assuming cores or the stability of the mean field. However, in their work [8], the effects of angular-momentum projections and three-body forces were approximately estimated by perturbative treatments.

Our aim is to make a systematic research on the structure of the ground and excited states of ^{11}Be based on the microscopic calculations. An important point is that the theoretical approach should be free from such model assumptions as stability of the mean field, and the existence of inert cores or clusters. First of all, traditional mean-field approaches are not useful to study the developed clustering structure in Be isotopes. With cluster models, the clustering structure of the excited states of ^{9}Be and ^{10}Be has been successfully explained [11,12,18–20] by assuming 2-α cores and surrounding neutrons. Since the assumption of 2 α-cluster cores is not appropriate to discuss the breaking of α-cores, these cluster models are not sufficient for investigations of ^{11}Be with many valence neutrons. In fact, it is difficult to use them to directly calculate the experimental data of the β-decay strength from ^{11}Li. With these models it may not be possible to describe the recently discovered excited state at 8.04 MeV with the strong β transition strength from ^{11}Li.

We have applied a theoretical approach of antisymmetrized molecular dynamics (AMD). The AMD method has already proved to be useful for studying the structures of light nuclei [8,10,21–24]. Within this framework, we do not need such model assumptions as inert cores, clusters, nor axial symmetries, because the basis wave functions of a nuclear system are written by Slater determinants where all centers of the Gaussian-type spatial part of single-particle wave functions are free parameters. In AMD studies of neutron-rich nuclei, we investigated the structures of Be isotopes [8,22,24]. In AMD calculations, many kinds of experimental data for nuclear structure have been reproduced. Due to the flexibility of the AMD wave function, we have succeeded to describe the structure changes between shell-model-like states and clustering states with an increase in the neutron number. In previous studies [8,22] on Be isotopes, the excited states of ^{11}Be were not studied in detail because the calculations are based on the variation before a total-angular-momentum projection. Recently, the AMD framework has been developed to be an extended version based on variational calculations after a spin-parity projection(VAP), which has already been confirmed to be powerful for studying the excited states of light nuclei. The method

has been applied to a stable nucleus ^{12}C [23], and to unstable nuclei: ^{10}Be, ^{12}Be and ^{14}Be [9,10,25].

In the present work, the structures of the ground and excited states of ^{11}Be were studied by performing VAP calculations using the AMD method. In the next section (Sec. II), we explain the formulation of AMD for a nuclear structure study of the ground and excited states. The adopted effective interactions are briefly explained in Sec. III. In Sec.IV, we present the theoretical results concerning the energy levels, β decays and $E2$ transitions compared with the experimental data. We predict a new rotational band with a well-developed clustering structure which comes from $2\hbar\omega$ configurations. In Sec.V, the intrinsic structure and behavior of the valence neutrons are discussed. We also discuss the breaking of α-clusters which has an important effect on the β-decay strength. Finally, we summarize our work in Sec. VI

II. FORMULATION

In this section, the formulation of AMD for a nuclear structure study of the excited states is explained briefly. For more detailed descriptions of the AMD framework the reader is referred to Refs. [10,22,23]

A. Wave function

An AMD wave function of a nucleus with mass number A is a Slater determinant of Gaussian wave packets;

$$\Phi_{AMD}(\mathbf{Z}) = \frac{1}{\sqrt{A!}}\mathcal{A}\{\varphi_1, \varphi_2, \cdots, \varphi_A\}, \tag{1}$$

$$\varphi_i = \phi_{\mathbf{X}_i}\chi_{\xi_i}\tau_i : \begin{cases} \phi_{\mathbf{X}_i}(\mathbf{r}_j) \propto \exp\left[-\nu\left(\mathbf{r}_j - \frac{\mathbf{X}_i}{\sqrt{\nu}}\right)^2\right], \\ \chi_{\xi_i} = \begin{pmatrix} \frac{1}{2} + \xi_i \\ \frac{1}{2} - \xi_i \end{pmatrix}, \end{cases} \tag{2}$$

where the ith single-particle wave function φ_i is a product of the spatial wave function ϕ_{X_i}, the intrinsic spin function χ_{ξ_i} and the isospin function τ_i. The spatial part ϕ_{X_i} is presented by a Gaussian wave packet whose center is defined by complex parameters X_{1i}, X_{2i}, X_{3i}. χ_{ξ_i} is the intrinsic spin function parameterized by ξ_i, while τ_i is the isospin function which is fixed to be up(proton) or down(neutron) in the present calculations. Thus an AMD wave function is parameterized by a set of complex parameters $\mathbf{Z} \equiv \{X_{ni}, \xi_i\}$ ($n = 1, 3$ and $i = 1, A$). $\mathbf{X}_i$ are the centers of Gaussians for spatial parts and the parameters ξ_i's determine the directions of intrinsic spins of the single particle wave functions.

If we consider a parity eigenstate projected from an AMD wave function, the total wave function consists of two Slater determinants,

$$\Phi(\mathbf{Z}) = (1 \pm P)\Phi_{AMD}(\mathbf{Z}), \tag{3}$$

where P is a parity projection operator. In the case of a total-angular-momentum projection(J-projection), the wave function of a system is represented by the integral of the rotated states,

$$\Phi(\mathbf{Z}) = P^J_{MK'}\Phi_{AMD}(\mathbf{Z}) = \int d\Omega D^{J*}_{MK'}(\Omega)R(\Omega)\Phi_{AMD}(\mathbf{Z}), \tag{4}$$

where the function D^J_{MK} is the well-known Wigner's D function and $R(\Omega)$ stands for the rotation operator with Euler angle Ω.

In principal the total wave function can be a superposition of independent AMD wave functions. For example, a system is written by a superposition of spin-parity projected AMD wave functions $P^{J\pm}_{MK'}\Phi_{AMD}$ as follows,

$$\Phi = cP^{J\pm}_{MK'}\Phi_{AMD}(\mathbf{Z}) + c'P^{J\pm}_{MK'}\Phi_{AMD}(\mathbf{Z}') + \cdots. \tag{5}$$

Expectation values of a given tensor operator T^k_q(rank k) for the total-angular-momentum projected states $P^{J_1\pm}_{M_1K_1}\Phi_{AMD}(\mathbf{Z})$ and $P^{J_2\pm}_{M_2K_2}\Phi_{AMD}(\mathbf{Z}')$ are calculated as follows,

$$\langle P^{J_1}_{M_1K_1}\Phi_1|T^k_q|P^{J_2}_{M_2K_2}\Phi_2\rangle \tag{6}$$

$$= \frac{2J_2+1}{8\pi^2}(J_2M_2kq|J_1M_1)\sum_{K\nu}(J_2Kk\nu|J_1K_1)\int d\Omega D^{J_2*}_{KK_2}(\Omega)\langle\Phi_1|T^k_\nu R(\Omega)|\Phi_2\rangle. \tag{7}$$

The three-dimensional integral can be evaluated numerically by taking a finite number of mesh points of the Euler angle Ω=(α,β,γ).

B. Energy variation

We make variational calculations for a trial wave function to find the state which minimizes the energy of the system;

$$\frac{\langle\Phi|H|\Phi\rangle}{\langle\Phi|\Phi\rangle}. \tag{8}$$

In the AMD framework, the energy variation is performed by a method of frictional cooling, one of the imaginary time methods. Regarding the frictional cooling method, the reader is referred to papers [21,22]. The time development of the parameters $\mathbf{Z}$ of a wave function $\Phi(\mathbf{Z})$ is simulated by the frictional cooling equations,

$$\frac{dX_{nk}}{dt} = (\lambda+i\mu)\frac{1}{i\hbar}\frac{\partial}{\partial X^*_{nk}}\frac{\langle\Phi(\mathbf{Z})|H|\Phi(\mathbf{Z})\rangle}{\langle\Phi(\mathbf{Z})|\Phi(\mathbf{Z})\rangle}, \quad (n=1,3 \quad k=1,A) \tag{9}$$

$$\frac{d\xi_k}{dt} = (\lambda+i\mu)\frac{1}{i\hbar}\frac{\partial}{\partial \xi^*_k}\frac{\langle\Phi(\mathbf{Z})|H|\Phi(\mathbf{Z})\rangle}{\langle\Phi(\mathbf{Z})|\Phi(\mathbf{Z})\rangle}, \quad (k=1,A) \tag{10}$$

with arbitrary real numbers λ and $\mu<0$. It is easily proved that the energy of the system decreases with each time step due to the frictional term:μ. After sufficient cooling iterations, the parameters for the minimum-energy state are obtained.

C. Wave function for $J^{\pm}$ states

In order to obtain the wave function for a $J^{\pm}$ state, we make the energy variation after a spin-parity projection(VAP) for an AMD wave function by using the frictional cooling method explained above. That is to say we perform the energy variation for the trial function $\Phi = P^{J\pm}_{MK'}\Phi_{AMD}(\mathbf{Z})$, the spin-parity eigenstate projected from an AMD wave function. First we make variational calculations after only the parity projection but before the spin projection(VBP) to prepare an initial trial wave function $\Phi_{AMD}(\mathbf{Z}_{init})$. After obtaining an initial wave function in VBP calculations we evaluate the expectation values of Hamiltonian for the spin-parity-projected states by choosing the body-fixed 3-axis for the Ω rotation to be the approximate principal z-axis on the intrinsic deformation. Then we find an appropriate K' quantum that gives the minimum diagonal energy of the spin-parity eigenstate

$$\frac{\langle P^{J\pm}_{MK'}\Phi_{AMD}(\mathbf{Z}_{init})|H|P^{J\pm}_{MK'}\Phi_{AMD}(\mathbf{Z}_{init})\rangle}{\langle P^{J\pm}_{MK'}(\mathbf{Z}_{init})|P^{J\pm}_{MK'}(\mathbf{Z}_{init})\rangle,} \tag{11}$$

where $K' = \langle J_3\rangle$. For each spin parity $J^{\pm}$, we start VAP calculations for the normalized energy expectation value $\langle P^{J\pm}_{MK'}\Phi_{AMD}(\mathbf{Z})|H|P^{J\pm}_{MK'}\Phi_{AMD}(\mathbf{Z})\rangle/\langle P^{J\pm}_{MK'}(\mathbf{Z})|P^{J\pm}_{MK'}(\mathbf{Z})\rangle$ with the adopted K' quantum from the initial state. In general, the direction of the approximately principal z-axis is automatically determined in the energy variation because the shape of the intrinsic system can vary freely. The approximately principal axis can deviate from the 3-axis in the VAP procedure with a given $K' = \langle J_3\rangle$. That is to say that the optimum state $P^{J\pm}_{MK'}\Phi_{AMD}$ obtained after the variation may contain so-called K-mixing ($K = \langle J_z\rangle$) components. However, the deviation of z-axis from the 3-axis is found to be small in many cases. It means that the obtained states do not contain K-mixing components so much, and K' well corresponds to the K quantum.

Concerning the states in the lowest band with each parity, we can obtain appropriate initial wave functions by simple VBP calculations as mentioned above. For the highly excited states, in order to obtain initial wave functions and appropriate K' quanta for VAP calculations we make VBP calculations with a constraint on AMD wave function. The details of the AMD calculation with constraints have been described in Refs. [21]. In the present calculations, we adopt a constraint as the expectation value of the total-oscillator quanta to equal with a given number. After choosing a corresponding K' quantum, we perform VAP calculations from the initial wave function. When we obtain other local minimum states than the obtained states, we consider them as the states in higher rotational bands.

D. Diagonalization

After the VAP calculations for $J^{\pm}_n$ states, the optimum intrinsic states $\Phi^1_{AMD}, \Phi^2_{AMD}, \cdots$, and Φ^m_{AMD} are obtained. Here m indicates the number of the calculated levels. we consider that the obtained wave functions approximately represent the intrinsic wave functions of the $J^{\pm}_n$ states. We determine the final wave functions by superposing the obtained AMD wave functions. That is to say that we determine the coefficients $c, c', \cdots$ in Eq. 5 for each $J^{\pm}_n$ state by diagonalizing the Hamiltonian matrix $\langle P^{J\pm}_{MK'}\Phi^i_{AMD}|H|P^{J\pm}_{MK''}\Phi^j_{AMD}\rangle$ and the norm matrix $\langle P^{J\pm}_{MK'}\Phi^i_{AMD}|P^{J\pm}_{MK''}\Phi^j_{AMD}\rangle$ simultaneously with regard to (K', K'') and (i, j). In comparison

with the experimental data such as the energy levels and the strength $E2$ transitions, the theoretical values are calculated with the final states after diagonalization.

III. INTERACTIONS

The adopted interaction for the central force is the case 3 of MV1 force [26], which contains a zero-range three-body term:$V^{(3)}$ in addition to the two-body interaction:$V^{(2)}$,

$$V_{DD} = V^{(2)} + V^{(3)} \tag{12}$$

$$V^{(2)} = \sum_{i<j}(1 - m + bP_\sigma - hP_\tau - mP_\sigma P_\tau) \left\{ V_A \exp\left[-\left(\frac{|\mathbf{r}_i - \mathbf{r}_j|}{r_A} \right)^2 \right] + V_R \exp\left[-\left(\frac{|\mathbf{r}_i - \mathbf{r}_j|}{r_R} \right)^2 \right] \right\}, \tag{13}$$

$$V^{(3)} = \sum_{i<j<k} v^{(3)} \delta(\mathbf{r}_i - \mathbf{r}_j)\delta(\mathbf{r}_i - \mathbf{r}_k), \tag{14}$$

where P_σ and P_τ stand for the spin and isospin exchange operators, respectively. As for the two-body spin-orbit force:V_{LS}, we use the G3RS force [27] as follows,

$$V_{LS} = \sum_{i<j} \{ u_I \exp(-\kappa_I r^2) + u_{II} \exp(-\kappa_{II} r^2) \} \frac{(1+P_\sigma)}{2} \frac{(1+P_\tau)}{2} \mathbf{l} \cdot (\mathbf{s}_i + \mathbf{s}_j), \tag{15}$$

$$\tag{16}$$

The Coulomb interaction:$V_{\rm C}$ is approximated by a sum of seven Gaussians. The total interaction V is a sum of these interactions: $V = V_{DD} + V_{LS} + V_C$.

IV. RESULTS

The structures of the excited states of ^{11}Be are studied based on the VAP calculations in the framework of AMD. In this section we present the theoretical results concerning the energy levels, the $E2$ transitions, and the β transitions, which should be directly compared with the experimental data. More detailed discussions of the intrinsic structures are given in the next section.

We adopt two sets of the interaction parameters. One parameter set (1) is $m = 0.65$, $b = h = 0$ for Majorana, Bartlett and Heisenberg terms in the central force and $u_I = -u_{II} =$ 3700 MeV for the strength of the spin-orbit forces, which have been used in the previous study on the excited states of ^{10}Be. We also try another set (2) with weaker spin-orbit forces as $u_I = -u_{II} = 2500$ MeV. Other parameters in the case (2) are same as those in the case (1). The width parameter ν is chosen to be 0.18 fm^{-2} which gives the minimum energy of ^{11}Be in a VBP calculation.

In VBP calculations we know that the lowest positive parity band $K^\pi = 1/2^+$consists of $1/2^+$, $3/2^+$,$5/2^+$,$7/2^+$ and $9/2^+$ states, and the lowest negative parity band $K^\pi = 1/2^-$ consists of $1/2^-$, $3/2^-$, and $5/2^-$ states. Therefore the $J^\pm_1$ states in the lowest bands are obtained by VAP calculations for $P^{J\pm}_{MK'}\Phi_{AMD}$ with the corresponding $(J^\pm, K')$ values as $(1/2^+, 1/2)$, $(3/2^+, 1/2)$, $(5/2^+, 1/2)$, $(7/2^+, 1/2)$, $(9/2^+, 1/2)$, $(1/2^-, 1/2)$, $(3/2^-, 1/2)$, $(5/2^-, 1/2)$. We calculate the higher excited states in the second negative parity band by VAP calculations with $(J^\pm, K')$= $(7/2^-, 3/2)$, $(9/2^-, 3/2)$, $(11/2^-, 3/2)$, $(13/2^-, 3/2)$, $\cdots$. These states are considered to belong to a band with $K^\pi = 3/2^-$. After obtaining the intrinsic states in

this second negative parity band for $J \geq 7/2$, the excited $J^{\pm} = 3/2^-_2$ and $5/2^-_2$ states in $K^{\pi} = 3/2^-$ are found as local minimums with VAP calculations by starting from the intrinsic states obtained for the higher spin states. In order to find the other excited $3/2^-$ state, we make VAP calculations for the spin-parity projected AMD wave function with the fixed intrinsic spin directions as 3 spin-down protons, one spin-up proton, 4 spin-down and 4 spin-up neutrons. The obtained wave function for the $3/2^-$ state is dominated by a component of total-intrinsic spin $S_p = 1$ for protons. We superpose the wave functions to calculate the final wave functions by diagonalizing Hamiltonian and norm matrixes simultaneously.

We should notice that all possible excited states are not exhausted in the present calculations. In this work we perform VAP calculations basically for the rotational states which can be known from VBP calculations with or without constraint. For the higher excited states we must extend the VAP calculations with orthogonal condition to the lower states by superpositions as the previous studies [10,23]. Above the states shown in the present results, there should exist other excited states which may be obtained with the extended VAP calculations.

A. Energies

The theoretical binding energies of ^{11}Be are 58.2 MeV in the case (1) and 54.4 MeV in the case (2), both of which underestimate the experimental value 65.48 MeV. The binding energy can be reproduced by choosing a interaction parameter such as $m = 0.60$ of the Majorana term. However unfortunately it is difficult to reproduce all the features of nuclear structures such as binding energies, energy levels, radii, deformations and so on with one set of interaction parameters. Since we study the excited states taking care about the excitation energies and the intrinsic structures, we adopt the case(1) interaction which reproduces well the features of the excited states of ^{10}Be [10] except for the binding energy. With this interaction the spin-parity $1/2^+$ of the ground state of ^{11}Be can be described in the present calculations. We also use another interaction case (2) with the weaker spin-orbit forces to be compared. The improvement of effective interactions is one of the important problems in nuclear studies.

Here we comment on the stability of AMD wave functions above threshold energies. Since the single particle wave functions are written by Gaussians in AMD calculations, the relative motion between particles in a system is restricted by a Gaussian or a linear combination of Gaussians. Because of the limitation of the model space, continuum states nor out going waves can not be represented in the present model. Even if the energy of a nucleus is above the threshold energies of particle decays, the particles can not necessarily go away in the present framework. In this sense, the system is treated in the bound state approximation. The widths for the particle decays should be discussed carefully by other frameworks such as the method with reduced width amplitude or the complex scaling method beyond the present AMD framework.

The energy levels of ^{11}Be are shown in Fig.1. There are many low-lying levels in the experimental data. The abnormal spin parity $1/2^+$ of the ground state has been known, although the normal spin parity of ^{11}Be is $1/2^-$ in the simple shell-model picture. The calculations with the case(1) interaction reproduce the parity inversion between $1/2^+$ and

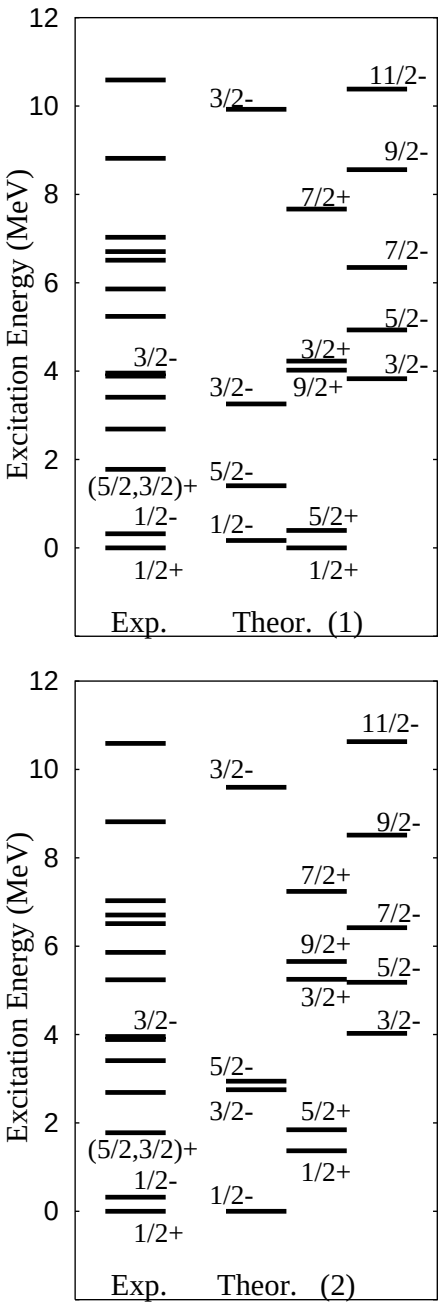

FIG. 1. The excitation energies of the excited states of ^{11}Be. Theoretical results with the case(1) and case(2) interactions are compared with the experimental data quoted from 'Table of Isotopes'.

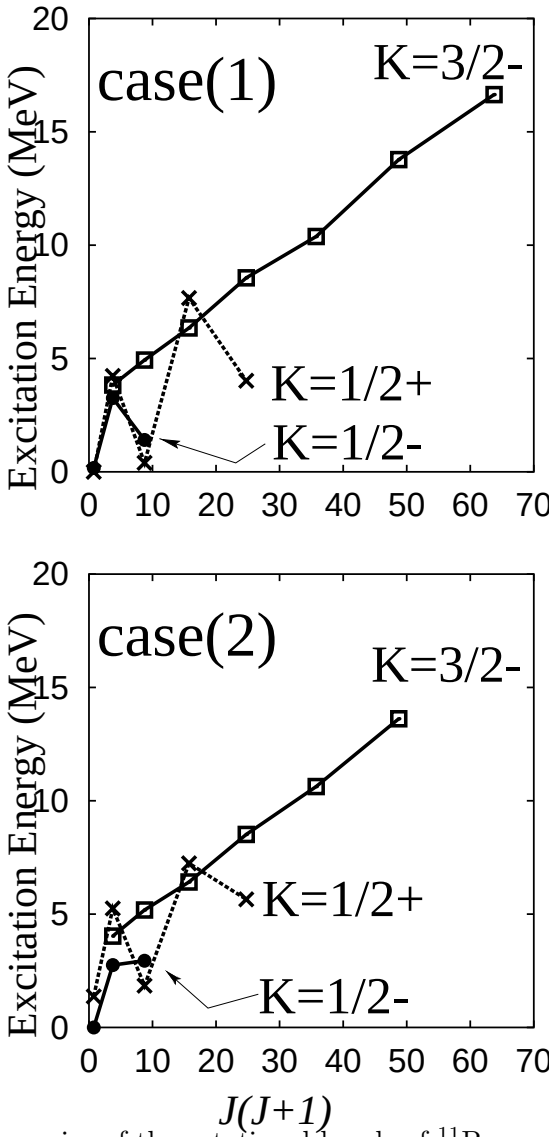

FIG. 2. The excitation energies of the rotational bands of ^{11}Be as a function of $J(J+1)$. The lines indicate the theoretically obtained rotational bands $K^\pi = 1/2^-$, $K^\pi = 1/2^+$, $K^\pi = 3/2^-$.

$1/2^-$ states. In the theoretical results, the rotational bands $K^\pi = 1/2^+$ and $K^\pi = 1/2^-$ start from the band head $1/2^+$ and $1/2^-$ states, respectively. Also in the results with the case(2) interaction, the $1/2^+$ state is lowest in the $K^\pi = 1/2^+$ band, however, it is slightly higher than the negative parity $1/2^-$ state by 1.4 MeV. As a result, the abnormal parity of the ground state can not be reproduced by the case (2) interaction which the spin-orbit forces are weaker than those in the case (1). We should not conclude the calculations with the case(1) interaction are better than those in the case (2), because the neutron halo effect on the energy gain of $1/2^+$ state is not taken into account in the present calculations. The details of the reproduction of parity inversion with the case(1) interaction are described in the later section.

In both results in the case (1) and the case (2), there exist some rotational bands in the low energy region. By classifying the calculated excited states we can obtain three rotational bands $K = 1/2^+$, $K = 1/2^-$ and $K = 3/2^-$ which are dominated by $1\hbar\omega$, $0\hbar\omega$ and $2\hbar\omega$ neutron configurations, respectively. In Fig.2, we show the excitation energies of the rotational bands as a function of total spin $J(J+1)$. We find a new eccentric band $K = 3/2^-$ which starts from the second $3/2^-$ state at about 4 MeV. The excited states in the $K = 3/2^-$ band are dominated by $2\hbar\omega$ excited configurations with 2 particles and 3 holes in neutron shells. The $K = 3/2^-$ band is constructed by a well-deformed intrinsic state with a developed clustering structure. The rotational band indicates large moment of inertia and it reaches the high spin states about 20 MeV. The highest spin is $15/2^-$ in the case (1) and $13/2^-$ in the case (2). In VAP calculations with further high spins, we can not obtain any stable states since an α particle escapes far away in the variational calculations. It means that the energy of the relative motion between clusters is beyond the classical barrier due to the coulomb and centrifugal forces. Since the barrier hight is very sensitive to the binding energy, we examine the highest spin of the $K = 3/2^-$ band with another set of the interaction parameters taking care of the binding energy of ^{11}Be. If we change the Majorana exchange term of case (1) to $m = 0.60$, we can make the system bound as deeply as the experimental binding energy. Then a $17/2^-$ state is obtained as the highest spin state. W. Von Oertzen et al. suggested some candidates for the states belonging to this new negative parity band in the experimental data observed in the 2 neutron transfer reactions, ^{9}Be(^{13}C, ^{11}C)^{11}Be [7]. Although they suggested a possibility of $19/2^-$ state, the present results are negative to such a high spin state as $19/2^-$ in the rotational $K = 3/2^-$ band, because $17/2^-$ is the highest spin made from the $2p$-$3h$ configurations. It should be noticed that the present work is the first microscopic calculation which predicts the $K^\pi = 3/2^-$ band with the well-developed clustering structure. Since ^{11}Be is a loosely bound system, further studies taking account of widths of the excited states are necessary to determine the band terminal.

We find a excited $3/2^-$ state at about 10 MeV (Fig 1). In this state, the proton structure is quite strange comparing with the other excited states of ^{11}Be. In most of the states of ^{11}Be, we find 2α cores as well as other Be isotopes: ^{8}Be, ^{9}Be and ^{10}Be. However, in the $3/2^-$ state at 10 MeV, only one α-cluster is formed. The other 2 protons do not form a α-cluster but couple to be totally $S = 1$ with aligned intrinsic spins. It is analogue with the structure of the first 1^+ state with the unnatural spin parity in ^{12}C. We consider that this $3/2^-$ state must be the newly measured state at 8.04 MeV [2] to which the β-decay transition from ^{11}Li is strong. Although its excitation energy is overestimated in the present calculations,

it is easily improved by changing parameters b and h of the Bartlett and Heisenberg terms. For example the parameters $b = -0.2$, $h = 0.4$, $m = 0.41$ gives 2 MeV lower excitation energy of the $3/2^-$ state than the one with $b = 0.0$, $h = 0.0$, $m = 0.65$. Here we fit the Majorana parameter m as to give the same α-α interaction as the case (1). The change of parameters gives no significant effect on the excitation energies of the other states with 2-α clusters. The results indicate that the Bartlett and Heisenberg terms should be taken into consideration in the detailed study of the energy levels though they have been often omitted in the traditional works on stable nuclei.

B. Transition strength

Data concerning the β-decay strength are very useful to investigate structures of excited states. There are many experimental data concerning the β^- and β^+ decays into the excited states of ^{11}Be. The strength of the β^- decays from ^{11}Li has been measured recently [2]. For the β^+ decays, the strength of Gamov-Teller(GT) transitions has been deduced from the charge exchange reactions ^{11}B(t,^{3}He)^{11}Be [3]. In the GT transitions from ^{11}Li($3/2^-$) and ^{11}B($3/2^-$), the allowed daughter states are $1/2^-$, $3/2^-$ or $5/2^-$ states. In Table I the experimental log(ft) values are presented comparing with the theoretical results. In order to calculate the log(ft) values of GT transistions into the excited states of ^{11}Be we prepare the parent states ^{11}Li($3/2^-$) and ^{11}B($3/2^-$) by VAP calculations in the same framework.

The experimental log(ft) values are reproduced well by the theoretical calculations. It is easily understood that the decays into the excited states in $K = 3/2^-$ band are weak because these states have the ell-developed clustering structures with dominated $2\hbar\omega$ components which make the overlap of a GT operator with the parent state of ^{11}B to be small. On the other hands, we consider that three levels at 0.32 MeV, 2.69 MeV and 3.96 MeV measured in the β^+ transitions correspond to the states $1/2^-_1$, $3/2^-_1$ and $5/2^-_1$ in the $K = 1/2^-$ band because the experimental data indicate the significant β^+ strength as log(ft) < 5.0, which consistent with the theoretical results.

What is important in the β^- decays from ^{11}Li is that the strength is very sensitive to the breaking of 2 α-cluster cores in ^{11}Be. If the daughter state of ^{11}Be poses 2 ideal α-cluster cores with $(0s)^4$ configurations, the GT transitions from ^{11}Li are forbidden completely because of Pauli principle. In another word, the strength of GT transitions from ^{11}Li indicates the degree of the α-cluster breaking in the daughter states of ^{11}Be. From this point of view, one of the reasons for the weak β^- transitions as log(ft)=5.67 to the lowest $1/2^-$ state at 0.32 MeV is the 2α-cluster structure in ^{11}Be($1/2^-$). Another reason for the weak β^- transitions has been suggested to be the effect of the halo structure in ^{11}Li by T. Suzuki et al. [28]. The ground state of ^{11}Li is known to have the neutron halo structure which originates from s-orbits. The mixing of the s-orbits causes weak β^- transitions to the normal states of ^{11}Be. Since the halo structure of ^{11}Li can not described in the present AMD wave function, the possible halo effects on the β^- decays are not included in the present results. If we suppose the mixing ratio of s-orbits in the ground ^{11}Li state as to be 50 %, the theoretical log(ft) values concerning the β^- decays into $1/2^-_1$, $3/2^-_1$ and $5/2^-_1$ is expected to be increased by log(2)$\sim$ 0.3 due to the mixing. Even if we add 0.3 of the halo effect by hands to the present log(ft) values for $3/2^-_1$ and $5/2^-_1$ states, the log(ft) values in case(1) are still smaller than

5.0, because of the sufficient cluster breaking. They are consistent with the experimentally measured rather small logft values for the decays to ^{11}Be(2.7 MeV) and ^{11}Be(3.9 MeV). In another word, the experimental data indicates the significant breaking of 2 α-cluster cores in these states(2.7MeV and 3.9MeV) which we consider as the excited states $3/2^-_1$ and $5/2^-_1$.

In the recent experiments of the measurements of β^- decays, a new excited state at 8.04 MeV with strong β^- transitions has been discovered. The calculated log(ft) values for the $3/2^-$ state of ^{11}Be at about 10 MeV well corresponds to this newly observed state at 8.04 MeV. The transition is strong because the 2α-cluster structure disappears completely in this state.

As shown in Table I, the experimental data concerning the strength of β^- decays have been systematically reproduced in the present calculations. Considering the increases of logft due to the halo effect of ^{11}Li, the theoretical values of logft for β^- calculated with the case (1) interaction well agree to the experimental data. The reason for the good reproduction is because the significant breaking of 2-α clusters in ^{11}Be is described in the present calculations. It is the same reason as the previous studies of ^{12}C in which the experimental data concerning the strength of β^- and β^+ decays have been well reproduced. The quantitative discussion of the 2α-core breaking will be given in the next section.

In Table II, we show the theoretical $B(E2)$ values. It has been proved that AMD calculations reproduce well $B(E2)$ values of light neutron-rich nuclei. As shown in the previous studies [9,22,23], the experimental Q-moments and $B(E2)$ values of various nuclei have been reproduced well by using the bare charges in the AMD framework because of the advantage of the AMD method which can directly describe proton deformations. Also in the present results, the features of proton-matter deformations in the intrinsic states are reflected in the theoretical $B(E2)$ values. In the lowest negative parity band $K^\pi = 1/2^-$, the intrinsic system deforms because of 2 α-cluster cores although the development of clustering is smallest comparing with the other bands. $B(E2)$ values are larger in the ground $K^\pi = 1/2^+$ band which has the developed clustering structure with a large deformation. The $B(E2)$ values are enhanced between the states in the second negative parity band $K^\pi = 3/2^-$ with an extremely large deformation due to the clustering development.

The $E1$ transition strength from $1/2^-_1$ to $1/2^+_1$ in ^{11}Be is known to be very large comparing with those in other light nuclei. The theoretical value of $B(E1; 1/2^-_1 \rightarrow 1/2^+_1)$=0.02 e·fm is much smaller than the experimentally observed strength 0.116 ± 0.011 e·fm. The halo structure may give an important effect on the $E1$ strength.

V. DISCUSSIONS

We investigate the structures of ^{11}Be focusing on the clustering aspects. It is found that two α-cluster cores are formed in most of the states of ^{11}Be as well as in other Be isotopes:^{8}Be, ^{9}Be, ^{10}Be. In the present calculations, we found three rotational bands with 2-α cores in ^{11}Be. In this section, we argue the development of clustering and investigate the roles of valence neutrons in the clustering states. We analyze the breaking of cluster cores and also describe the feature of a non-clustering state. The problem of parity inversion between positive and negative parity states is also discussed.

TABLE I. Log(ft) values of the β transitions. The theoretical values are obtained from the Gamow-Teller transition strength. The experimental data of β decays from ^{11}Li are taken from Ref. [2]. Logft values concerning the Gamow-Teller transition from ^{11}B are deduced from the charge exchange reactions [3].

transitions	logft theory (1)	theory (2)
^{11}Li$(3/2^-) \rightarrow ^{11}Be(1/2^-_1)$	5.0	5.5
^{11}Li$(3/2^-) \rightarrow ^{11}Be(3/2^-_1)$	4.4	5.0
^{11}Li$(3/2^-) \rightarrow ^{11}Be(5/2^-_1)$	4.5	5.0
^{11}Li$(3/2^-) \rightarrow ^{11}Be(3/2^-_2)$	4.9	6.2
^{11}Li$(3/2^-) \rightarrow ^{11}Be(3/2^-_3)$	3.9	4.3
^{11}B$(3/2^-) \rightarrow ^{11}Be(1/2^-_1)$	3.9	4.2
^{11}B$(3/2^-) \rightarrow ^{11}Be(3/2^-_1)$	3.8	4.3
^{11}B$(3/2^-) \rightarrow ^{11}Be(5/2^-_1)$	4.2	5.0
^{11}B$(3/2^-) \rightarrow ^{11}Be(3/2^-_2)$	4.5	5.5
^{11}B$(3/2^-) \rightarrow ^{11}Be(3/2^-_3)$	4.3	5.4
transitions	exp.	
^{11}Li$(3/2^-) \rightarrow ^{11}Be(1/2^-_1$, 0.32 MeV)	5.67(4)	
^{11}Li$(3/2^-) \rightarrow ^{11}$Be(2.69 MeV)	4.87(8)	
^{11}Li$(3/2^-) \rightarrow ^{11}$Be(3.96 MeV)	4.81(8)	
^{11}Li$(3/2^-) \rightarrow ^{11}$Be(5.24 MeV)	5.05(8)	
^{11}Li$(3/2^-) \rightarrow ^{11}$Be(8.04 MeV)	4.43(8)	
transitions	exp.	
^{11}B$(3/2^-) \rightarrow ^{11}Be(1/2^-_1$, 0.32 MeV)	4.3(1)	
^{11}B$(3/2^-) \rightarrow ^{11}$Be(2.69 MeV)	4.4(1)	
^{11}B$(3/2^-) \rightarrow ^{11}$Be(3.96 MeV)	4.8(2)	

TABLE II. $E2$ strength of ^{11}Be. The theoretical results of AMD with the interactions case(1) are listed.

transitions	present results (e^2 fm^4)
^{11}Be;$3/2^-_1 \to 1/2^-_1$	9
^{11}Be;$5/2^-_1 \to 1/2^-_1$	8
^{11}Be;$5/2^-_1 \to 3/2^-_1$	2
^{11}Be;$5/2^-_2 \to 3/2^-_2$	37
^{11}Be;$7/2^-_1 \to 3/2^-_2$	14
^{11}Be;$7/2^-_1 \to 5/2^-_2$	25
^{11}Be;$5/2^+_1 \to 1/2^+_1$	14
^{11}Be;$5/2^+_1 \to 3/2^+_1$	7
^{11}Be;$3/2^+_1 \to 1/2^+_1$	13
^{11}Be;$5/2^-_2 \to 3/2^-_1$	7
^{11}Be;$3/2^-_2 \to 3/2^-_1$	8
^{11}Be;$3/2^-_2 \to 1/2^-_1$	2

A. Clustering structure

We investigate the intrinsic structures of the excited states focusing on the clustering aspects. Although the states $P^{J^\pm}_{MK}\Phi^i_{AMD}$ are superposed for all the obtained wave functions Φ^i_{AMD} so as to diagonalize a Hamiltonian matrix, the $J^\pm$ state after the diagonalization is found to be dominated by the AMD wave function $P^{J^\pm}_{MK}\Phi^j_{AMD}$ which is obtained in a VAP calculation for the given spin and parity $J^\pm$. Therefore we consider an obtained AMD wave function Φ_{AMD} with a VAP calculation as the intrinsic wave function of the corresponding $J^\pm$ state.

In the excited states, three rotational bands: $K = 1/2^+$, $K = 1/2^-$ and $K = 3/2^-$ are recognized, because the intrinsic structures of the states in each band are similar. The density distributions of the intrinsic states of the band head states: $1/2^-_1$, $1/2^+_1$ $3/2^-_2$ are shown in Fig.3. The neutron structure of an intrinsic state is very different from the ones of the other rotational bands. The density distributions of neutrons are presented in the right column in Fig.3. As for the neutron deformation, the $1/2^-$ state has an oblate deformation. The oblate shape is natural for the normal parity state in a system with the neutron number $N = 7$. In the positive parity $1/2^+$ state, the neutron density deforms prolately. The prolate deformation of neutron density is extremely enhanced in the $3/2^-_2$ state. The detailed discussions of neutron structures is given later by analyzing the single-particle behavior of neutrons.

In the proton density shown in the middle column in Fig.3, we can see dumbbell shapes due to 2 pairs of protons. Roughly speaking, it indicates that 2-α cores are formed in all the intrinsic states of these three rotational bands. The spatial development of clusters is small in the lowest negative parity $1/2^-_1$ state which has a main component of a normal $0\hbar\omega$ configuration. In the ground $1/2^+$ state with the abnormal parity, the 2α clustering structure develops. It is interesting that the most remarkable clustering structure is seen

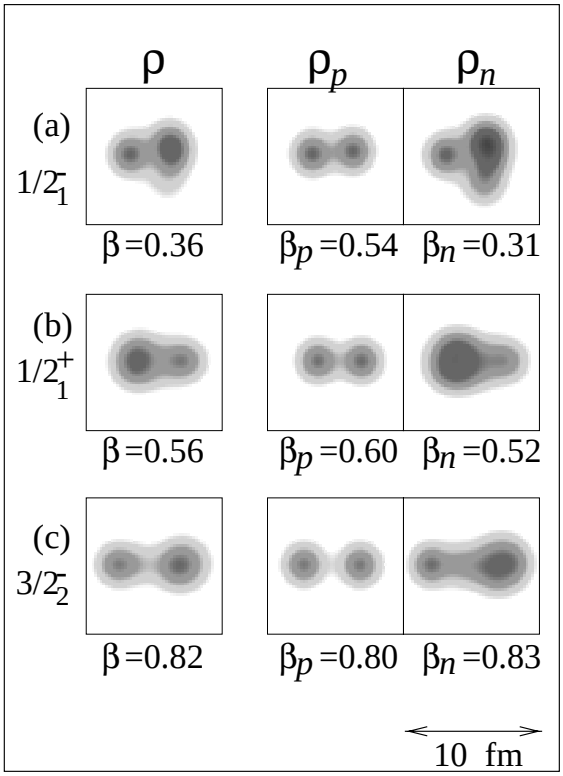

FIG. 3. The density distributions of the intrinsic structures of $1/2^-_1$, $1/2^+_1$, $3/2^-_2$ states calculated with the case(1) interaction. The intrinsic system is projected on to a plain which contains the longitudinal axis of the intrinsic states. The density is integrated along a transverse axis perpendicular to the plain. The density distributions for matter, proton and neutron are presented in the left, middle and right, respectively.

in the $3/2^-_2$ state which belongs to the $K = 3/2^-$ band. In this state, the relative distance between 2-α cores is largest among these 3 rotational bands. It seems that the 2α-clustering structure develops following the prolate deformation of neutron density. According to the development of 2α clustering, the proton deformation is larger in the $K = 1/2^+$ band than in the $K = 1/2^-$ band, and largest in the $K = 3/2^-$ band. The difference of the proton structures are reflected in the theoretical $B(E2)$ values as mentioned in the previous section. Namely, the theoretical values concerning the strength $B(E2)$ are large in the transitions between the states in the rotational bands with the large proton deformations. As mentioned above, the $K = 3/2^-$ band is the largely deformed state with the well development clustering structure. However, the deformation decreases and the clustering weakens at the band terminal state with the increase of spin near the highest spin $J = 15/2^-$ in case(1).

B. Behavior of valence neutrons

As mentioned in the previous subsection, the deformation of neutron density changes drastically between the rotational bands. We inspect the single-particle wave functions of the intrinsic states to study the behavior of valence neutrons. The single-particle wave functions of an intrinsic state are obtained by transforming from the original Gaussian

functions to the orthonormal single-particle wave functions under the diagonal condition of the single-particle Hamiltonian matrix. The definition of single-particle wave functions and energies of an AMD wave function is described in Refs. [8,10].

In Be isotopes, it has been known that the molecular orbits around 2α play important roles. The molecular orbits in Be isotopes have been suggested in ^{9}Be with $2\alpha + n$ cluster models [19]. W. Von Oertzen et al. proposed a picture of Be dimers [6,7] to understand the excited states of neutron-rich Be isotopes. They predicted σ- and π-orbits which are made from linear combinations of p-orbits surrounding 2-α clusters (see Fig.4). Itagaki et al. have described the structures of ^{10}Be and ^{12}Be with a extended cluster model by assuming α cores and the molecular orbits. In the study of Be isotopes with AMD methods [8,9,22], the structures with 2 αs and valence neutrons in neutron-rich Be isotopes have been microscopically confirmed without assuming the existence of any clusters nor molecular orbits. In the present work we investigate the behavior of the valence neutrons focusing on the molecular orbits.

By analyzing the ratio of positive and negative parity components in each single-particle wave function, it is found that all the neutron orbits are approximately parity-eigen states, which roughly correspond to $1s$-, $1p$-, and $2s1d$ orbits. The lowest normal-parity $1/2^-$ state comes from a $0\hbar\omega$ configuration because 2 neutrons occupy s-like orbits and the other 5 neutrons are in p-like orbits. On the other hand, in the ground $1/2^+$ state with the abnormal parity, the last neutron occupies a sd-like orbit, which means that the $1/2^+$ state is dominated by a $1\hbar\omega$ configuration. An interesting feature is found in the highest neutron wave function which well corresponds to the sd-like orbit. The density distribution of neutrons are presented in Fig.5(a). It has nodes along the longitudinal direction of 2-α clusters and contains nearly 90% of a positive-parity eigen state. It well corresponds to the so-called molecular σ-orbit explained in the schematic figure 4(a). On the other hand, the features of 2 neutron orbits energetically below the σ-orbit are shown in 4(b). The dominating negative-parity component of these orbits indicates that the orbits correspond to the p-like orbits. As shown in Fig.5(b), the orbits seem to be similar to the molecular π-orbits.

One of the reasons for parity inversion of ^{11}Be is considered to be because of the molecular σ-orbit which originates from sd-orbits. Since Be isotopes prefer to prolate deformations because of 2-α clusters, the σ-orbit can easily gain its kinetic energy in the clustering developed system. In another word, the 2α-clustering structure is one of advantages for the σ-orbit in Be isotopes. From this point of view, it is easy to understand the reason for the clustering development in the $1/2^+_1$ state in terms of the energy gain of the σ-orbit in a clustering system. Figures 6(a),(b),(c) show the single-particle energies in the intrinsic states of $1/2^-_1$, $1/2^+_1$ and $3/2^-_2$ with the case (1) interaction, respectively. The highest orbit in Fig.6(b) corresponds to the σ-orbit in $1/2^+_1$ state. The energy of the intruder σ-orbit is lower than the highest π-orbit in $1/2^-_1$. In all the states:$1/2^-_1$, $1/2^+_1$ and $3/2^-_2$, the 2-α cores consist of 4 neutrons and 4 protons in the $1s$-like orbits and the lower p-like orbits seen in Fig.6. The behavior of the single-particle wave functions of valence neutrons in the present results is almost consistent with the previous AMD studies [8,30].

One of new discoveries in the present work is that the possible negative-parity band $K = 3/2^-$ has a largely deformed shape with a remarkable clustering structure. With the same analysis of the single-particle wave functions as mentioned above, we find that 2 neutrons in the $3/2^-_2$ state occupy so-called σ-orbits. In another word, the well-developed

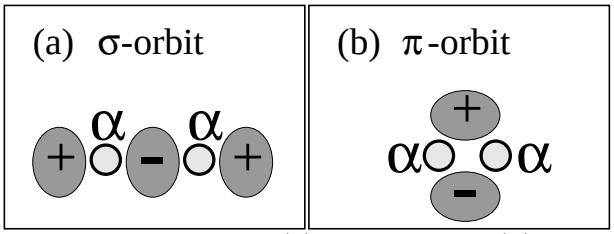

FIG. 4. Sketches for the molecular orbits, (a) σ-orbits and (b)π-orbits surrounding 2αs. The molecular orbits are understood by linear combinations of p-shell orbits around the α clusters.

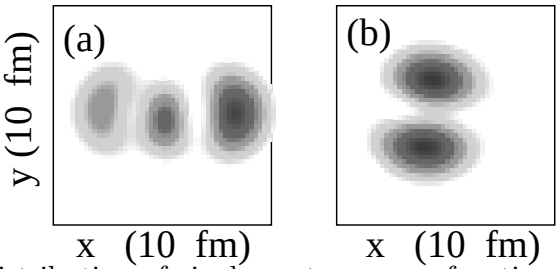

FIG. 5. The density distribution of single-neutron wave functions in the intrinsic system of $1/2^+_1$ state calculated with case (1). Figure (a) shows the density for the highest neutron orbit with 90% positive parity component, while figure (b) is for the second neutron orbit which contains 90% of a negative parity component.

clustering is caused by these 2 neutrons in the σ-orbits so as to gain their kinetic energies. It is surprising that such a 2 $\hbar\omega$ state appears in the low energy region. The clustering structure in the $K = 3/2^-$ band is the very molecular structure which has been predicted by W. Von Oertzen [7]. This is the first microscopic calculation which shows that such an exotic structure should exist in the low energy region.

In the single-particle energies shown in Fig.6(c), we find another interesting thing that the energies of the σ-orbits in $3/2^-_2$ state become lower than that of an odd neutron π-orbit. One of reasons for the higher energy of the odd neutron π-orbit than the σ-orbits is a lack of the pairing interaction because of the absence of the other neutron in the π-orbit. Another reason is the degeneration between σ-orbits and π-orbits at the large inter-cluster distance. With the increase of relative distance between 2-α clusters, the σ-orbits gain their energy, while the π-orbits loose their potential energies. As the relative distance increases, the σ-orbits cross the higher π-orbits and come down near the lower π-orbits. It is helpful to see the neutron level scheme of two center shell model [31] to understand the inversion of π- and the σ-orbits with the increase of inter-cluster distance.

In the single-particle energies shown in Fig.6, the small level spacing between the lower $1s$-orbits and the lower $1p$-orbits indicates the development of 2 α clusters in $1/2^+$ and $3/2^-_2$ states. In fact, the level spacing is smallest in $3/2^-_2$ state.

As mentioned above, we see the drastic change of neutron structures between three rotational bands. It is found that the origins of drastic change are the neutrons in σ-orbits and π-orbits surrounding 2-α cores. The intrinsic states are characterized by the number of valence neutrons in the σ-orbit. That is to say that, no neutron, one neutron and two neutrons occupy the σ-orbits in the $K = 1/2^-$ $K = 1/2^+$ $K = 3/2^-$ bands, respectively. The deformation with clustering structure is enhanced by the increase of the neutrons which

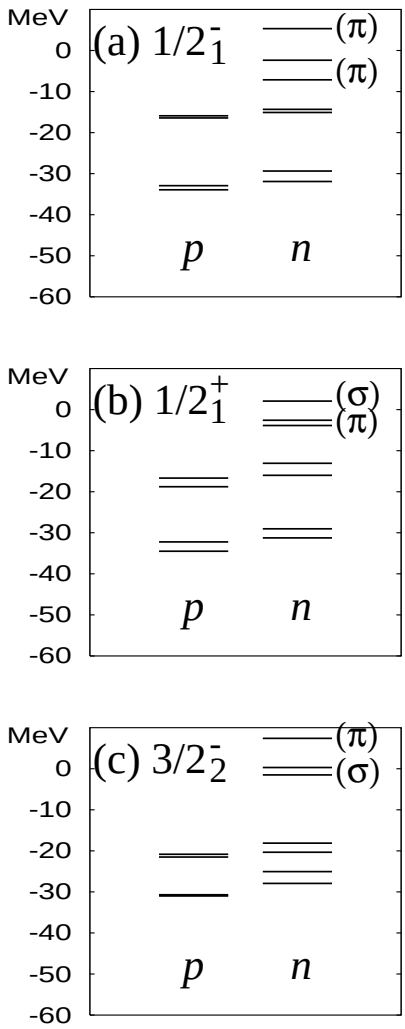

FIG. 6. Single-particle energies in the intrinsic system of (a)$1/2^-_1$, (b)$1/2^+_1$, (c)$3/2^-_2$ with the case (1) interaction. Energies for protons(neutrons) are presented in left(right) in each figure.

occupy the σ-orbits due to the energy gain of σ-orbits in the developed clustering structure.

C. Breaking of 2α cluster cores

Although the structures with 2 α-cluster cores are seen in most of the states of ^{11}Be, the α clusters are not the ideal α clusters with simple $(0s)^4$ configurations. The α clusters are broken slightly because of the spin-orbit force. The components of cluster breaking allows the β decays from ^{11}Li into ^{11}Be. This is a similar situation as seen in the 3α-cluster structures of ^{12}C to which Gamow-Teller transitions from ^{12}B and ^{12}N are not weak.

In the calculated results, we can know the degrees of breaking from the ideal 2-α clusters by estimating non-zero total-intrinsic spin($S_p \neq 0$) components for protons. If we neglect $S_p \geq 2$ components and assume that only $S_p = 0$ and $S_p = 1$ components are contained in a state, the value $0.5 \times \langle S_p^2 \rangle$ indicates directly the mixing ratio of the non-$(0s)^4$ configurations, which signifies the degrees of cluster breaking in the state. In table III, the expectation values of the squared total-intrinsic spin of protons are listed. Generally speaking, the clustering breaking is larger in the results in the case (1) than in the case (2) because the stronger spin-orbit forces in the case (1) give larger effects on the dissociation of 2 α-cluster cores. The states $1/2_1^-$, $3/2_1^-$ and $5/2_1^-$ in $K = 1/2^-$ contain significant components of the cluster breaking in the ratios of 7%, 10% and 20%, respectively. The mixing of cluster breaking allows the β decays into these states from ^{11}Li, which consistent with the experimental measurements (Table.I). The smaller mixing in $1/2_1^-$ than the other $3/2_1^-$, $5/2_1^-$ states is reflected on the relatively weak β decays to $1/2_1^-$ as mentioned in the previous section on the β-decay strength. On the other hand, the breaking of α clusters are very small in $K = 1/2^+$ and $K = 3/2^-$ which have the well-developed clustering structures. Therefore Gamow-Teller transitions to the excited states in $K = 3/2^-$ band from ^{11}Li are predicted to be weak except for the β decays to the $3/2_2^-$ state because this state slightly contains the cluster breaking due to the state mixing with the lower $3/2_1^-$ state.

We discover an excited $3/2_3^-$ state where the 2α-cluster structure is completely broken. In the density distribution of protons we can not recognize the dumbbell shape in this state (see Fig.7). As seen in Table III, the main component is the proton intrinsic spin $S_p = 1$ state. As a result, the β-decay transitions from ^{11}Li to the $3/2_3^-$ state are strong comparing with the β-decay strength to the other excited states of ^{11}Be. It is consistent with the strong β decays to the state at 8.04 MeV, which have been recently measured.

Although the 2α-core structures are dominant in most of Be isotopes, it is interesting that the excited state with the completely breaking of one of 2 αs appears in neutron-rich Be. Even in the excited states with 2-α cores, the components of the cluster breaking play an important role in the strength of β decays from ^{11}Li.

D. parity inversion

We consider details of parity inversion of the ground state in the case(1) calculations. Concerning the energy gain of the positive parity $1/2^+$ state, the effects of the halo structure, the clustering structure with a prolate deformation, the three-body force, the angular-momentum projection, and the paring have been discussed in the pioneering works [16].

TABLE III. The expectation values of the squared total intrinsic spin of protons S_p^2 in the excited states of ^{11}Be.

$J_n^{\pm}$ states	$0.5 \times \langle S_p^2 \rangle$	
	case(1)	case(2)
($K = 1/2^-$ band)		
$1/2_1^-$	0.07	0.04
$3/2_1^-$	0.1	0.04
$5/2_1^-$	0.2	0.04
($K = 3/2^-$ band)		
$3/2_2^-$	0.04	0.003
$5/2_2^-$	0.01	0.003
$7/2_2^-$	0.01	0.002
($K = 1/2^+$ band)		
$1/2_1^+$	0.03	0.01
$3/2_1^+$	0.02	0.01
$5/2_1^+$	0.03	0.01
$7/2_1^+$	0.02	0.01
$9/2_1^+$	0.02	0.004
$3/2_3^-$	0.7	1.0

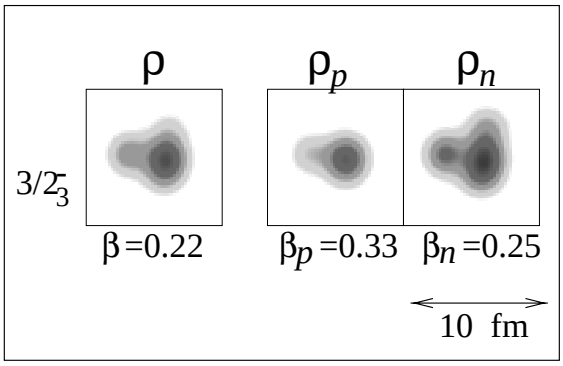

FIG. 7. The density distribution of the intrinsic wave function of $3/2_3^-$ calculated with the case(1) interaction.

In the present calculations the effects of clustering structure are included as well as the pioneering AMD studies [16,22]. One of the reasons for parity inversion is the energy gain of the molecular σ-orbit in the system with developed 2α clustering. The details of clustering and molecular orbits have been already mentioned above.

The three-body force was calculated approximately with a perturbative treatment in the pioneering study [16]. In the present work, the three-body force is treated exactly as same way as the previous AMD study in Ref. [22].

In the previous AMD studies of ^{11}Be [16,22], the angular-momentum projection was perturbatively treated. That is to say that the energy variation was performed after a parity projection but before an angular-momentum projection(VBP). In the present results, we perform energy variation exactly for the spin-parity projected wave functions(VAP). Then we find that the effect of angular-momentum projection on the parity inversion is quite different from the previous VBP results with perturbative treatments. In order to quantitatively discuss the effects, we estimate the energy difference between $1/2^-$ and $1/2^+$ states: $\delta E \equiv E_{1/2^+} - E_{1/2^-}$. The parity inversion is described by a negative value of δE. The experimental value of δE has been known to be -0.32 MeV. For simplicity we do parity-projected AMD calculations with fixed intrinsic spins by using the case(1) interaction. In table IV, the values of δE and energies (a) without angular-momentum projections, (b) the angular-momentum projections after variation within the perturbative treatments of VBP, and (c) results of the exact VAP calculations are listed. Before the angular-momentum projections, δE is 0.6 MeV. After the projection within the perturbative treatments of VBP, δE becomes small as -1.1 MeV. It is because that the energy gain of the positive-parity state by the angular-momentum projection is 1.7 MeV larger than the gain of the negative-parity state. The origin is the well-developed clustering structure in the former state comparing with the latter state because a deformed system gains much energy due to a angular-momentum projection in general. The VBP results are consistent with the previous AMD studies in Refs. [22,16]. However when we exactly treat the angular-momentum projection with VAP calculations we find a new aspect in the effects on the energy gain. In the previous AMD studies, it is known that in many cases VAP results of low-lying states is not so much different from VBP results. It is true in the $1/2^+$ state. However it is not true in the $1/2^-$ state. In the VAP calculations, the negative parity state gains much energy as 8.6 MeV due to the angular-momentum projection because the deformation of $1/2^-$ state grows more largely in the VAP calculations than in the VBP calculations so as to gain the energy of the angular-momentum projected state. As a result, δE of (c) is 1.0 MeV as much as the result before projections (a). In fact, the clustering of ^{11}Be$(1/2^-_1)$ is larger in the VAP results than as is expected in the VBP calculations. Therefore the effect of the angular-momentum projection is not positive for the parity inversion in ^{11}Be. This is one of new things in the present work which points that the perturbative treatments of angular-momentum projections do not always work well for precise descriptions.

Comparing with the previous AMD studies of low-lying states of ^{11}Be [16,22], another improvement in the present framework is treating the intrinsic spin functions as variational parameters. In the TableIV, the effect of the flexible intrinsic spins are seen in the difference between (c) the VAP calculations with the fixed intrinsic spins and (d) the VAP calculations with the variational intrinsic spins. The treatment of flexible intrinsic spins gives an important effect on the parity inversion of ^{11}Be. It reduces δE to a 1.1 MeV smaller value

TABLE IV. Energies of the positive and negative parity states of ^{11}Be. The parity projected AMD calculations with fixed intrinsic spins (a) before angular-momentum projections, (b) after angular-momentum projections of VBP within the perturbative treatment, and (c) results of the exact VAP calculations are listed. We also show (d) the present VAP calculations with variational intrinsic spins but no diagonalization of the basis. The adopted interactions are the case(1) force. The energy difference δE between the positive and negative parity states is defined as $E_{1/2^+} - E_{1/2^-}$ for the calculations after angular-momentum projections and $E(+) - E(-)$ before the projection.

	(a) before projection	(b) VBP	(c)VAP	(d)VAP
intrinsic spins	fixed	fixed	fixed	variational parameters
^{11}Be(+)	-46.5	-53.1	-54.7	-57.1
^{11}Be($-$)	-47.1	-52.0	-55.7	-57.0
δE	0.6	-1.1	1.0	-0.1

in (d) than that in the calculations (c). The importance of the flexible intrinsic spins in $p_{3/2}$ shell-closure states has been already argued in the studies of ^{12}C [23] by one of the authors. In the case of ^{11}Be, it is natural to consider that the $p_{3/2}$ sub-shell effect is one of the reasons for the parity inversion because the $p_{1/2}$-orbit sould be raised relatively higher than $2s_{1/2}$-orbits. Unfortunately, the simple AMD method with the fixed intrinsic spins describe the sub-shell effects insufficiently. This is one of the advantages of the present framework which can describe well both aspects of the clustering and shell effects.

Regarding the other reasons of parity inversion, Sagawa et al. [14] and Doté et al. [16] suggested the paring effects in the neutron p-shell. In the present framework, a part of the paring effects in p-shell should be included automatically by the spin-parity projections and the superpositions.

As mentioned above, the clustering effects, the three-body forces, the $p_{3/2}$ sub-shell effects are included in the present calculations. The paring effects are expected to be partially contained. The other effect which should be important for parity inversion is the neutron-halo effect [13,16]. According to the study in Ref. [16], the effect due to the neutron halo structure is estimated as 0.6 MeV reduction of δE. However the halo effect is not taken into account in the present calculations. We think that this halo effect and the residual paring effect are contained effectively in the strength parameter $u_{LS} = 3700$ MeV of the spin-orbit force which is slightly stronger that the parameter $u_{LS} = 3000$ MeV adopted in Ref. [23]. The halo structures should be important only for the loosely bound states with low-spin orbits such as s-orbits and p-orbits at most. The present strong effective spin-orbit force in case(1) may artificially reduce too much the theoretical excitation energies of the other states in $K = 1/2^+$ band except for the $1/2^+$ state. Before concluding the relative position of the energies between $K = 1/2^-$ and $K = 1/2+$ bands we should more detailed researches by taking the remained effects such as the halo structure into consideration.

VI. SUMMARY

We studied the structures of the ground and excited states of ^{11}Be with VAP calculations in the framework of antisymmetrized molecular dynamics. Various kinds of excited states with the clustering structures and also the non-clustering structures were discovered in the theoretical results. We predicted many excited states. Most of the states belong to three rotational bands: $K = 1/2^+$, $K = 1/2^-$ and $K = 3/2^-$, which are dominated by $1\hbar\omega$, $0\hbar\omega$ and $2\hbar\omega$ configurations, respectively. It should be pointed out that the formation of 2 α-cluster cores is seen in many excited states of ^{11}Be in the the present resutls in spite of no assumption of the existence of clusters. The interesting point is that an eccentric rotational band $K = 3/2^-$ with the mostly developed clustering structure starts from the $3/2^-_2$ state at about 4 MeV and reaches high spin states.

The experimental data concerning the β^+-decay and β^--decay strength were reproduced well. We also argued that the cluster breaking plays an important role to allow the β decays from ^{11}Li. The significant breaking of 2-α cores in the states in $K = 1/2^-$ band has been seen in quantitatively estimating the breaking of clusters. We discovered a non-clustering state at about 10 MeV. One of the characteristics of this state is the strong β decays from ^{11}Li, which well corresponds to the new excited states at 8.04 MeV found in the β^--decay measurements.

By analyzing the single-particle wave functions in the intrinsic states, it was found that the molecular σ-orbits surrounding 2-α cores play important roles in the clustering structures of ^{11}Be. In the ground band $K = 1/2^+$, one neutron occupies the σ-orbits. In the newly predicted $K = 3/2^-$ band is dominated by $2\hbar\omega$ configurations with two neutrons in the σ-orbit. When the surrounding neutrons occupy the σ-orbits, the clustering development is enhanced so as to gain their kinetic energy. In another word, one of the reasons for the parity inversion and the low-lying $2\hbar\omega$ states is the energy gain of the σ-orbits with the developed clustering structures.

Concerning the mechanism of the parity inversion, we described the importance of molecular neutron orbits in the developed clustering structure and also mentioned about the $p_{3/2}$ sub-shell effect. Although the spin parity of the ground state is described with a set of interaction parameters case (1), we need more detailed researches taking the halo structures of the ground state into account.

ACKNOWLEDGMENTS

The authors would like to thank Dr. N. Itagaki and Dr. Doté for many discussions. They are also thankful to Professor W. Von Oertzen for helpful discussions and comments. The computational calculations of this work are supported by the Supercomputer Project No.58, No.70 of High Energy Accelerator Research Organization(KEK), and Research Center for Nuclear Physics in Osaka University.

REFERENCES

[1] A. A. Korsheninnikov et al., Phys. Lett. B **343**, 53 (1995) .
[2] N. Aoi, et al., Nucl. Phys. A**616** 181c (1997).
[3] I. Daito, et al., Phys. Lett. B **418** 27 (1998).
[4] M. Freer et al., Phys. Rev. Lett. **82**, 1383 (1999); M. Freer et al., Phys.Rev.**C63**, 034301 (2001).
[5] M. Milin et al., Europhys. Lett. 48, 616 (1999).
[6] W. von Oertzen, Z. Phys. A **354**, 37 (1996); W. von Oertzen, Z. Phys. A **357**, 355 (1997).
[7] H. G. Bohlen, et al. IL NUOVO CIMENTO Vol.**111A, N.6-7**, 841 (1998).
[8] A. Doté, H. Horiuchi, and Y. Kanada-En'yo, Phys. Rev. C **56**, 1844 (1997).
[9] Y. Kanada-En'yo, H. Horiuchi and A. Doté, J. Phys. G, Nucl. Part. Phys. **24** 1499 (1998).
[10] Y. Kanada-En'yo, H. Horiuchi and A. Doté, Phys. Rev. **C 60**, 064304(1999).
[11] N. Itagaki and S. Okabe, Phys.Rev.C61:044306,(2000); N. Itagaki, S. Okabe and K. Ikeda, Phys.Rev.**C 62**034301,(2000).
[12] Y. Ogawa, K. Arai, Y. Suzuki, K. Varga, **A673**, 122, (2000).
[13] H. Sagawa, Phys. Lett. **B286** (1992), 7.
[14] H. Sagawa, B. A. Brown and H. Esbensen, Phys. Lett. **B309 (1993)**, 1.
[15] T. Otsuka, N. Fukunishi, and H. Sagawa, Phys. Rev. Lett. **70**, 1385 (1993).
[16] A. Doté and H. Horiuchi, Prof. 103, 91 (2000).
[17] I. Ragnarsson, S. Aberg, H. B. Kansson and R. K. Sheline, Nucl. Phys. **A361** (1981), 1.
[18] M. Seya, M. Kohno, and S. Nagata, Prog. Theor. Phys. **65**, 204 (1981).
[19] S. Okabe, Y. Abe, and H. Tanaka, Prog. Theory. Phys.**57**, 866(1977); S. Okabe, Y. Abe, Prog. Theory. Phys.**61**, 1049(1979)
[20] K. Arai, Y. Ogawa, Y. Suzuki, K. Varga, Phys.Rev.**C54** 132(1996).
[21] Y. Kanada-En'yo and H. Horiuchi, Prog. Theor. Phys. **93**, 115 (1995).
[22] Y. Kanada-En'yo, A. Ono, and H. Horiuchi, Phys. Rev. C **52**, 628 (1995); Y. Kanada-En'yo and H. Horiuchi, Phys. Rev. C **52**, 647 (1995).
[23] Y. Kanada-En'yo, Phys. Rev. Lett. **81**, 5291 (1998).
[24] Y. Kanada-En'yo and H. Horiuchi, Prog. Theor. Phys. Suppl.**142**, 205(2001).
[25] Y. Kanada-En'yo, Proc. of the Yukawa Internatinal Seminar 2001, Kyoto, Nov 2001, to be published in Prog. Theor. Suppl.
[26] T. Ando, K.Ikeda, and A. Tohsaki, Prog. Theor. Phys. **64**, 1608 (1980).
[27] N. Yamaguchi, T. Kasahara, S. Nagata, and Y. Akaishi, Prog. Theor. Phys. **62**, 1018 (1979); R. Tamagaki, Prog. Theor. Phys. **39**, 91 (1968).
[28] T. Suzuki and T. Otsuka, Phys. Rev. C **50** R555, (1994)
[29] E. K. Warburton and B. A. Brown, Phys. Rev. C **46**, 923(1992).
[30] Y. Kanada-En'yo, Docter thesis (1996).
[31] J. M. Eisenberg and W.Greiner, *Nuclear Theory I* (North-Holland, Amsterdam, 1975) , p.571.